

Electrophoretic preparation of a Cu/Graphene composite as a Field Emitter with Enhanced Properties

Leifeng Chen^{1,*}, Hua Yu¹, Jun Wu^{2*}

¹ College of Materials and Environmental Engineering, Hangzhou Dianzi University, Hangzhou 310018, China

² Institute of Electron Device & Application, Hangzhou Dianzi University, Hangzhou, Zhejiang 310018, China

*E-mail: chlf@hdu.edu.cn (L. Chen) and wujun@hdu.edu.cn (J. Wu)

Received: 18 January 2020 / Accepted: 21 March 2020 / Published: 10 July 2020

To optimize the field emission behavior of graphene, a simple, low-cost and large-scale method was developed to introduce metallic particles onto the graphene and is described in the present report. Cu/graphene composite field emitters were fabricated by the one-step process of electrophoretic deposition. The Cu/graphene composite emitters prepared with this technique showed a lower turn-on electrode of 1.55 V/ μm , lower threshold field of 2.45 V/ μm and higher field enhancement factor of 5600 compared with those of the pristine graphene. The optimized field emission properties of the Cu/graphene composite were mainly attributed to the introduced Cu nanoparticles, which increased the density of the emission sites and decreased the series resistance. These results provide us with a new approach to optimize graphene-based emitters for vacuum devices.

Keywords: Graphene, Field emission, Cu nanoparticles, composite

1. INTRODUCTION

Graphene has drawn additional attention in this decade due to its exceptional physical, chemical and mechanical properties [1,2]. Due to its high aspect ratio, abundant sharp edges, large surface-to-volume ratio, and excellent electrical and thermal conductivity, graphene is expected to be a promising material for fabricating high-performance vacuum devices [3-5]. The additional wrinkled edges can allow electrons to easily tunnel through the surface potential barrier under a low external electronic field [6]. Research progress in recent years for graphene and graphene-based composites/hybrids has given rise to an increased interest in this field [7-9]. Graphene or graphene-based composites/hybrid field emission devices can be fabricated by many methods. However, most graphene field emission devices experience challenges because the sheets are often assume a flat position on the substrate. Graphene field emission mainly resulted from the edges of single-layer graphene in previous reports [10,11]. By creating

additional emission sites on the surface of a graphene sheet, the voltage for electron emission from the graphene sheets can be reduced [12]. Although the graphene edges contributed additional electrons for field emission, the low number of emitting sites limited the emission current density. Currently, graphene emitters exhibit high resistance and degraded mechanical performance during the field emission process [13-15]. The high contact barrier/resistance between graphene and the substrate limits the high current density of the field emission devices. To improve the electrical conductivity, a substantial amount of effort has been expended by different groups by the fabrication of composite materials [16,17].

The characteristics of graphene-based composite/hybrid materials include a new structural nature and additional synergistic performance. Composite systems can display better properties than their individual segments [18-20]. Graphene-based composites/hybrids can improve the performance of graphene, such as its electrical, mechanical, and thermal properties [21,22]. The composites/hybrids have mutually complementary structures and properties. Therefore, they have expanded potential applications in electronic devices, especially in vacuum devices [23-26]. The Electrophoretic deposition (EPD) process is a fascinating technique for the operation and management of nanomaterials, especially carbon-based materials. The deposition parameters can be easily controlled, and the morphological conformation of the materials have considerable flexibility. For the EPD method, the quantity and quality of deposition can be accurately manipulated. The EPD technique requires a simple apparatus, has a high deposition rate, and is economical, convenient and inexpensive. In recent years, graphene field emitters have been successfully fabricated by EPD. Because the EPD technique has a high deposition rate and throughput, it is an economical, convenient and inexpensive process, but the graphene sheets are generally flatly laid on the substrate surface by EPD. The small number of emitting locations limits the emission current from the graphene emitters. To optimize the field emission performance, composites/hybrids of graphene with metal nanoparticles have received a substantial amount of attention in recent years [27,16,17]. Compared with the properties of pristine graphene, the nanoparticle/graphene composites/hybrids showed an improvement. Composites of graphene and metal nanoparticles exhibit a synergistic effect, so a low turn-on field, low threshold field, high enhancement factor and good emission stability can be obtained.

In this work, a Cu/graphene composite was fabricated by a one-step method that introduced copper metallic particles. The Cu/graphene composite emitters showed a low turn-on electric field and high current density. The optimized field emission performance was analyzed and is discussed.

2. EXPERIMENTAL

In this experiment, in order to build the Cu/graphene composite field emitter by one step method, the electrophoretic deposition (EPD) technique is adopted and the schematic diagram is presented in Figure 1. For preparing electrophoretic solution, analytically pure isopropyl alcohol (IPA) was served as the organic solvent. And then 5 mg graphene powder was put into 200 ml IPA. In order to make the Cu^{2+} ions absorbed on graphene sheets surface, the $\text{Cu}(\text{NO}_3)_2 \cdot 3\text{H}_2\text{O}$ at an initial concentration of $1 \times 10^{-4} \text{M}$ was dissolved in IPA. For obtaining the homogeneous graphene electrophoresis suspension, the above mixture solution was placed in a sonic bath for 3 h. After cooling down for the graphene electrophoresis

suspension at room temperature, the silicon wafer and the Cu sheet were put into the suspension. The Si substrate connected to the negative electrode while Cu sheet connected to the positive one, which the two electrodes were kept with distance of about 1cm. The deposition process was employed by keeping a constant DC voltage of 100 V and the deposition time was maintained in 15 min. Under the electric field force, the graphene sheets covered on Cu^{2+} ions can be driven to move towards the negative electrode of Si substrate. When graphene sheets adsorbed by Cu^{2+} ions arrived at the negative electrode, the Cu^{2+} ions can be reduced to form metallic Cu particles. At the same time, the atoms of Cu sheet could lose two negative electrons to form Cu^{2+} ions and then the Cu^{2+} releases into the IPA solution. The concentration of the Cu^{2+} in electrophoresis suspension can be kept constant during the EPD process. Soon after finishing EPD process, the Cu/graphene composite film on Si substrate is rinsed in IPA and deionized water thoroughly, respectively. For getting the strong adhesion with the Si substrate, the Cu/graphene samples were annealed at 200–400°C in nitrogen atmosphere for about 1 h.

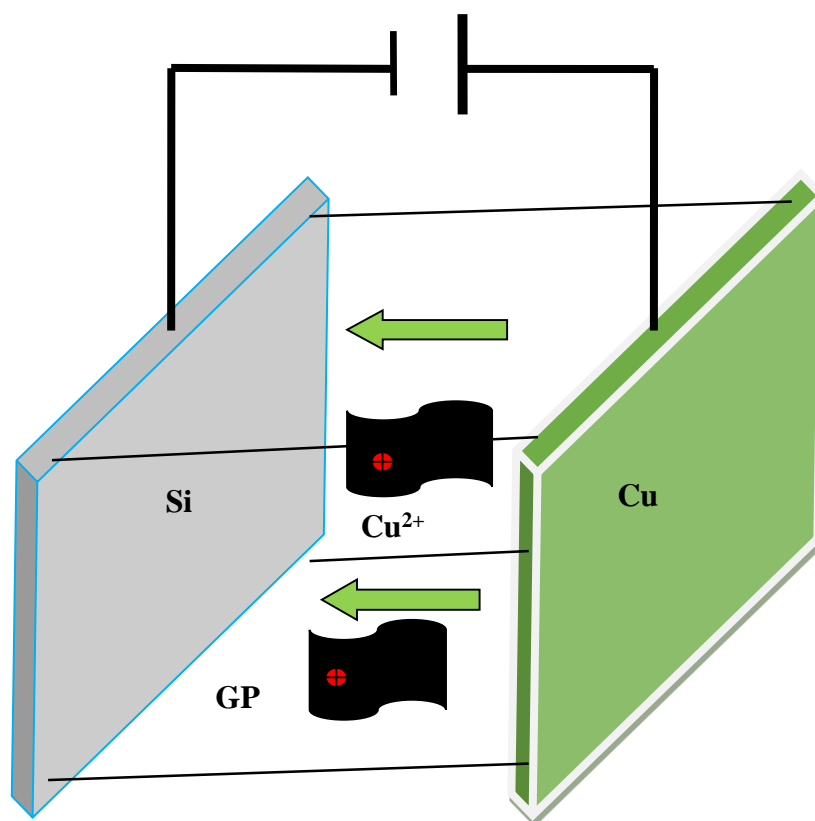


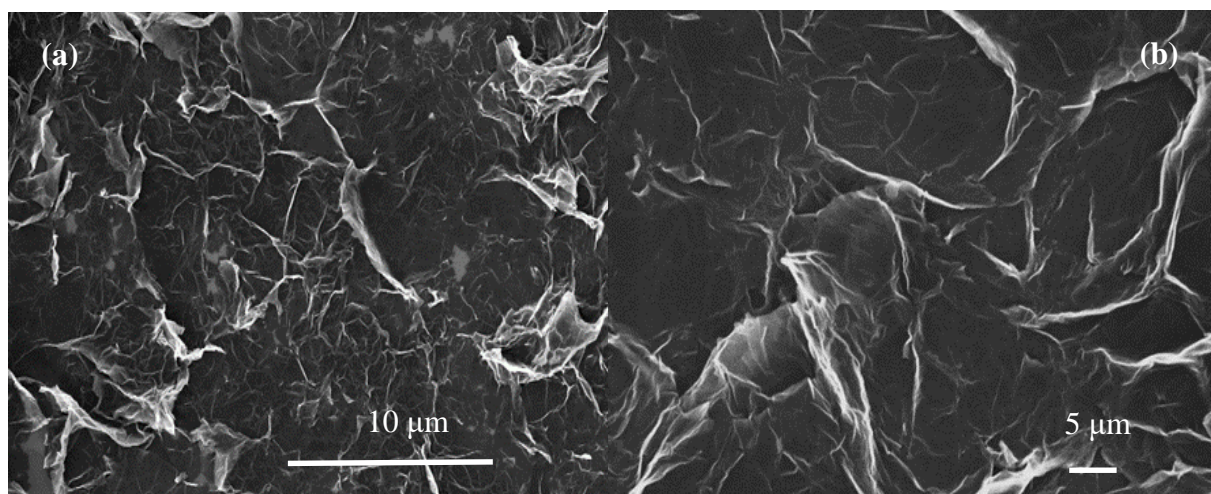
Figure 1. Schematic diagram of the EPD device for fabrication of Cu/GP composite.

In order to characterize and analyze the Cu nanoparticles/graphene composite and pristine graphene surfaces morphologies, the scanning electron microscopy (SEM, Hitachi SU-70), transmission electron microscope (TEM) and high-resolution transmission electron microscope (HRTEM) were used as the tools. The micro-Raman spectrometer was used to characterize the Raman spectra, which were recorded in backscattering geometry. The excitation wavelength of the Ar ion laser was 514.5 nm. The FE characteristics were tested with the diode structure, which the Cu/graphene composite emitters and

a Si substrate were used as the cathode and the anode respectively. During the measurement, the vacuum chamber was maintained at a pressure of 1×10^{-5} Pa at room temperature. Direct voltage was applied to the anode and the emission current was also measured at the anode. The emission current was measured using an Agilent electrometer (Model 34401A). The cathode was grounded, and the anode was positively biased during the measurement process. For short circuit protection, a resistance in series was connected in the circuit. For the analysis of the FE behavior, the turn-on field (E_{to}) and the threshold field (E_{th}) were defined as the electric fields required to produce a current density of $10 \mu\text{A}/\text{cm}^2$ and $1 \text{mA}/\text{cm}^2$, respectively.

3. RESULTS AND DISCUSSION

Figure 2(a) and (b) show the morphologies of the pristine graphene film on a Si substrate fabricated by EPD observed with SEM at low and high magnifications. In the low-magnification image, it can be seen that the graphene sheets were attached to the Si substrate. Parts of the graphene sheet tips protruded from the Si substrate. In the high-magnification image, it can be clearly seen that the edges of the graphene were extended from the Si substrate. The extended edges can possess a high aspect ratio. These sharp edges can enhance the local electric field and play a key role in electron field emission. Figure 2(c) shows an SEM image of the Cu nanoparticle/graphene composite fabricated by the one-step EPD method. Many Cu nanoparticles decorated the graphene sheets, and the Cu nanoparticles were uniformly distributed on the graphene sheets. In the high-magnification image, we can see that Cu nanoparticles that coated on graphene sheets were in the range of 10-40 nm. Prominent Cu nanoparticles can magnify the local electric field of the graphene sheets or tips, and they can also act as additional emission sites.



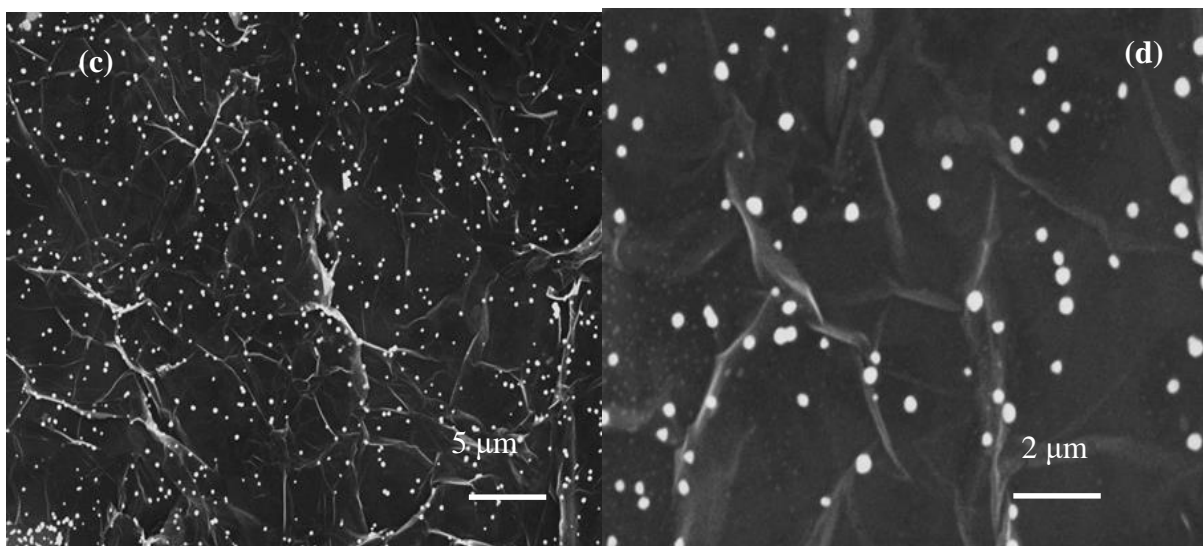


Figure 2. SEM images of the GP emitter at low (a) and high magnifications (b). SEM images of the Cu/GP composite field emitter fabricated by EDP at low (c) and high magnifications (b).

The Cu nanoparticles can further connect the graphene sheets with the Si substrate. This connection can increase the contact area and decrease the contact resistance, and the contact area determines the contact resistance between the Cu nanoparticle/graphene composite and Si substrate. Thus, the electrons could be easily tunneled from the interface barrier to emitters [28, 29], which is discussed in detail later.

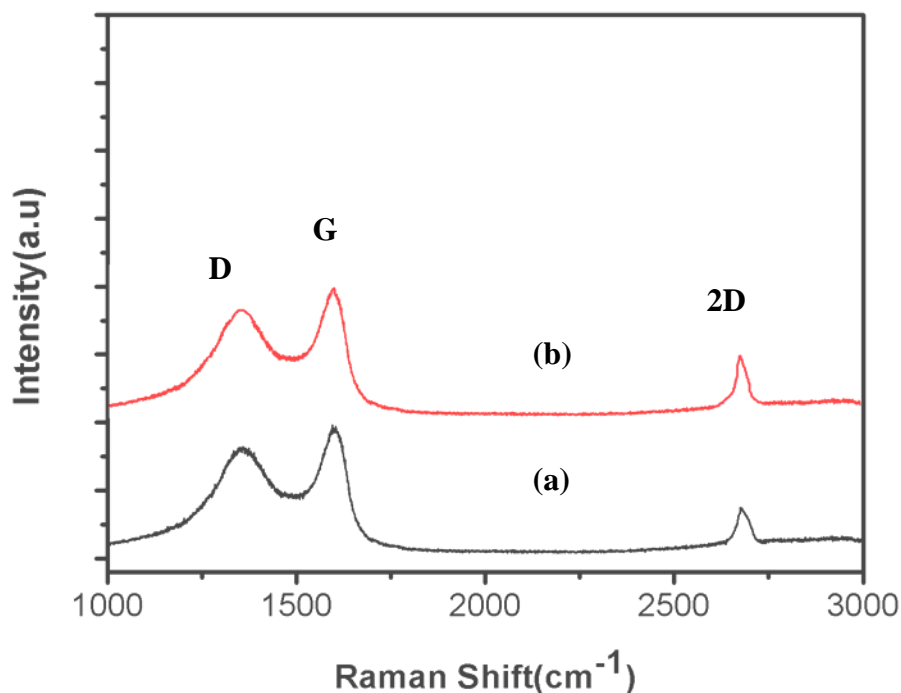


Figure 3. Raman spectra of the pristine graphene (a) and Cu/graphene composite (b).

Raman spectroscopy was used to characterize the structure and electronic properties of the graphene and Cu nanoparticle/graphene composite. Figure 3 shows the Raman spectra of pristine graphene and the Cu/graphene composite. The D (1350 cm^{-1}), G (1582 cm^{-1}) and 2D (2700 cm^{-1}) bands for both the graphene and composite clearly appeared. The D band shifted, and the intensity of the D band for the Cu/composite showed almost no change after the copper metallic particles were introduced to the graphene sheets. The copper nanoparticles on the graphene sheets did not cause essential changes in the Raman spectrum, which is consistent with the results in previous reports [30, 31].

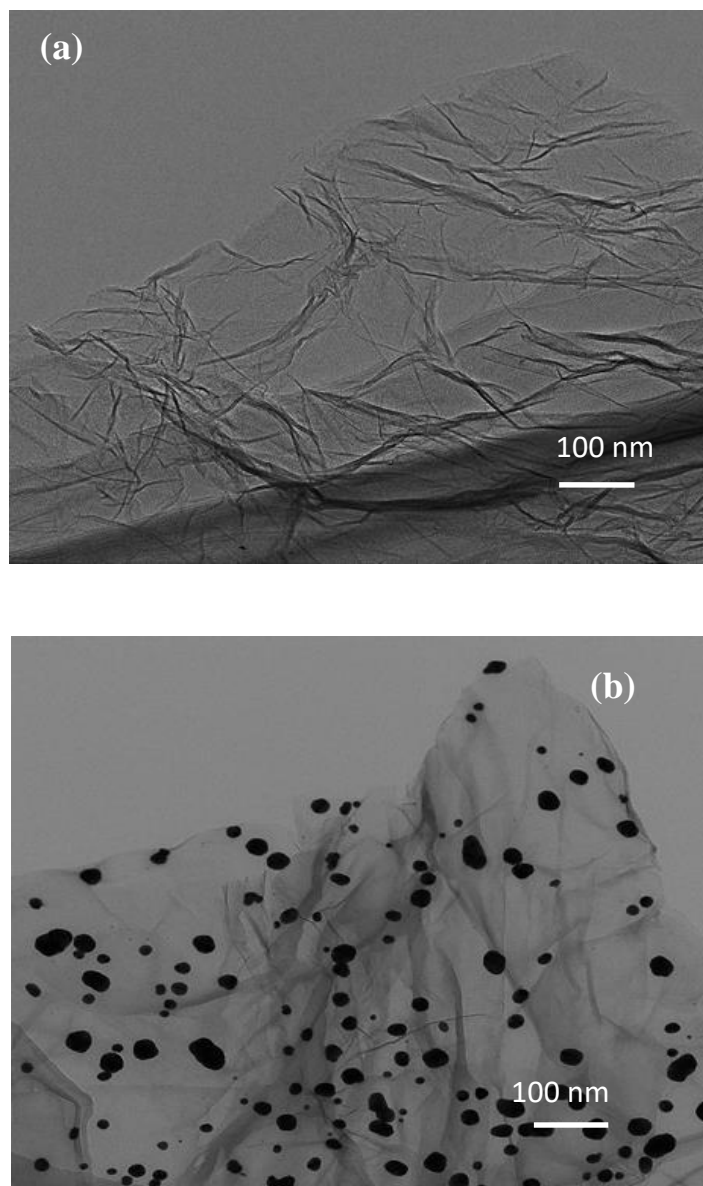


Figure 4. TEM images of the pristine GP (a) and Cu nanoparticle/graphene composite (b)

A TEM image, shown in Figure. 4(a), indicates that the surface of the pristine graphene sheet was corrugated and the film was transparent. This TEM image shows that the pristine graphene sheet was clear and did not contain other residues. After the one-step fabrication of the Cu

nanoparticle/graphene composite, a large number of Cu nanoparticles decorated the surface of the graphene sheets and had a size range of 10-40 nm, as shown in Figure 4(b).

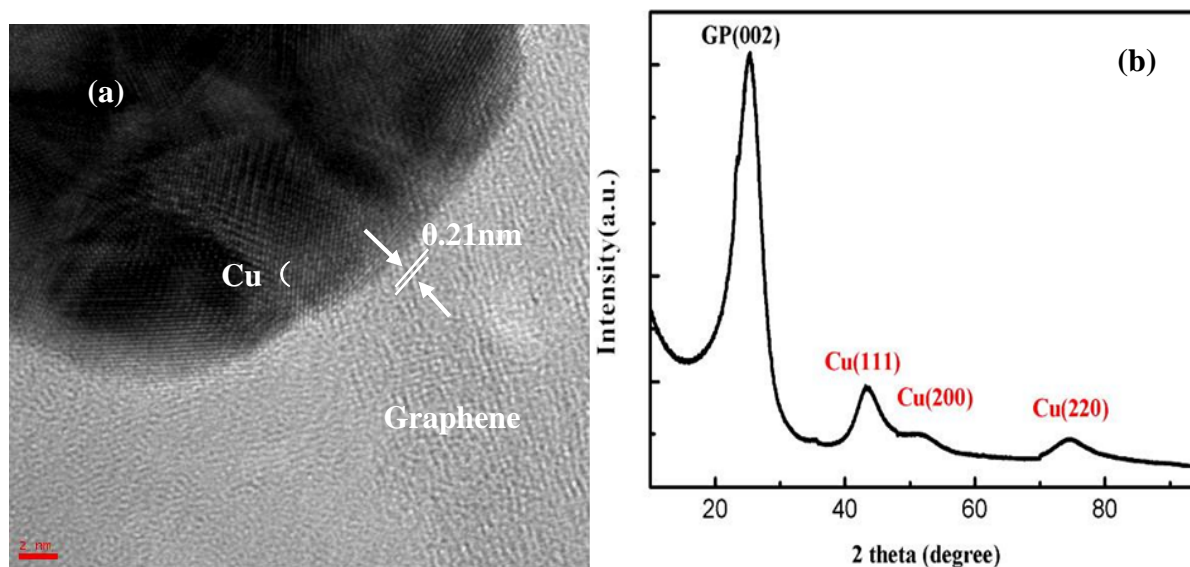


Figure 5. HRTEM image (a) and X-ray diffraction (XRD) pattern (b) of the Cu/graphene composite.

HRTEM and X-ray diffraction (XRD) were carried out to prove that the Cu particles coated the surface of the graphene sheets. The HRTEM image shown in Figure 5a confirmed that the Cu nanoparticles had a typical crystalline nature with a lattice spacing of 0.21 nm, corresponding to the planes of face-centered cubic (fcc) Cu [32-34]. The Cu nanoparticles made intimate contact with the graphene sheets, providing evidence for the formation of Cu/graphene composite heterostructures. Therefore, it was verified that Cu^{2+} ions were reduced to metallic Cu during the EPD process. The XRD pattern of the Cu/graphene composite is presented in Figure. 5(b). The dominant peak at $2\theta = 24.0^\circ$ is observed, which corresponds to the (002) planes of graphitized graphene. The other three characteristic peaks at $2\theta = 43.5^\circ$, 50.8° , and 74.6° correspond to the (1 1 1), (2 0 0), and (2 2 0) planes of fcc Cu, respectively [35,36]. The XRD patterns further confirmed the reduction of the Cu^{2+} ions during the EPD process.

Figure 6 shows the curves of the extracted emission current density versus the applied electric field ($J-E$) for the Cu/graphene composite and pristine graphene. After fabricating the graphene/Cu composite by the one-step method that introduces copper metallic particles onto graphene sheets, the E_{to} was reduced from 2.25 to 1.55 V/ μm . The E_{th} at the current density was considerably reduced from 2.86 to 2.45 V/ μm . The field emission performance of the Cu/graphene composites were improved significantly in comparison with that of the pristine graphene. The $\ln(J/E^2)$ versus $1/E$ (F-N plots) plots corresponding to the Cu nanoparticle and pristine graphene emitters are displayed in the inset of Figure 6. The F-N plots show approximately linear behavior, which indicated that the emitting electrons escaped from the surface barrier tunneling.

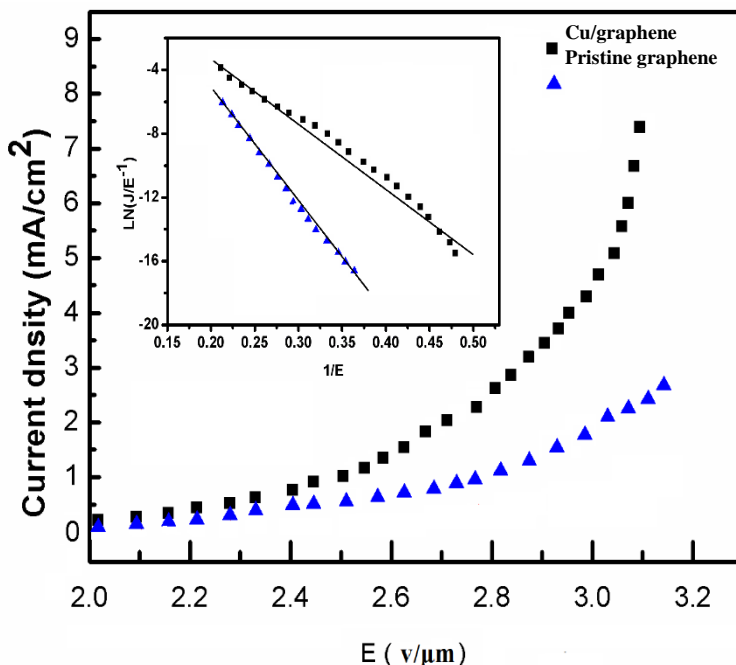


Figure 6. J–E curves of the Cu/graphene composite and pristine graphene, and the inset contains the corresponding F–N plots.

Field emission characteristics are generally investigated by the Fowler and Nordheim (F-N) theory [37]. This model has been extensively used for the electron quantum tunneling mechanism, which describes electrons that escape from the cathode material and travel to the anode through a vacuum surface barrier under an external electrical field. According to the F-N law, the relationship between the field emission current density J and the applied electric field E is presented as follows:

$$J = \eta a \frac{(\beta E)^2}{\phi} \exp\left(-b \frac{\phi^{3/2}}{\beta E}\right) \tag{1}$$

where J is the macroscopic emission current density; ϕ is the work function of the cathode materials in eV; a and b are constant coefficients of $1.54 \times 10^{-6} \text{ A eV V}^{-2}$ and $6.83 \times 10^3 \text{ eV}^{-3/2} \text{ V}^{-1} \mu\text{m}$, respectively; η describes the geometrical efficiency of the electron emission; and β is the field enhancement factor. β describes the relationship between the applied and local electric field where electron quantum tunneling occurs. E is the applied macroscopic electrical field between the cathode and anode, and E usually equals V/d . Here, V and d are the voltage and distance between the cathode and anode, respectively. According to the slope of the F-N plot (k_{FN}), we can calculate the enhancement factor β with the following equation:

$$\beta = b \phi^{3/2} / k_{FN} \tag{2}$$

where K_{FN} represents the slope of the F - N plot. The work function for graphene is assumed to be equal to that of graphite (5.0 eV). We can calculate the value of K_{FN} for composite and pristine graphene from the slopes of the F - N plots. The enhancement factors for the Cu/graphene composite and pristine graphene were estimated to be approximately 5600 and 3650, respectively. This β value for the composite is higher than that of the pristine graphene. The high field enhancement factor for the Cu/graphene composite was concluded to be from the graphene sharp edges and Cu nanoparticles that decorated on the graphene. The Cu nanoparticles on the graphene sheets added additional emission sites. The Cu nanoparticles formed many raised and sharp tips on the graphene sheets, which resulted in an enhanced local field in the raised regions. Therefore, the large β value for the Cu/graphene composite enabled easy tunneling of the electrons from the raised regions of the emitters, which resulted in an optimized field emission.

The two crucial parameters for field emission are the work function ϕ and field enhancement factor β , where the field emission current density increases with β and decreases with ϕ . However, the whole field emission process can also be controlled by the series resistance, especially the interface contact and the emitter resistance [38, 39, 29]. We can determine the overall electron field emission process from the following factors. During the first step, the electrons cross over the substrate to the emitter materials and overcome the contact barrier or resistance between the substrate and the field emitter. During the second step, the electrons are transported through the field emitter and finally tunnel into the vacuum from the surface of the field emitter. From the above electron transport process, we can see that the contact barrier/resistance and resistance of the emitter play a vital role in the field emission process. Therefore, we measured the resistances of the Cu/graphene composite emitter and pristine graphene using four-probe measurements. The contact resistances between the emitter and substrate were also measured by the four-wire measurement method according our previous report on Ag/graphene hybrid emitters [40-42]. The pristine graphene resistance and contact resistance were 300 Ω /sq and 1.5 Ω /mm², respectively. The resistance and contact resistance for the Cu/graphene composite were 245 Ω /sq and 0.32 Ω /mm², respectively. From these results, we can see that the resistance and interface contact resistance were reduced after fabricating the Cu/graphene composite. Thus, as the series resistance decreased, the interface between the substrate and composite supplied enough electrons to pass through and then tunnel through the surface barrier easily.

The improvement in the contact resistance between the emitter and substrate by the introduction of Cu particles can also be described as follows. The wettability of the graphene was improved by Cu nanoparticles supported on the graphene sheets. As the wettability of the graphene increased, the contact area between the emitter and substrate increased. Therefore, the contact resistance between graphene and the Si substrate was reduced by increasing the contact area with the substrate.

We can calculate the contact resistance r_c from the formula below, where the r_c of the graphene sheets decorated with Cu nanoparticles is [43]:

$$r_c = \left(\frac{\kappa_B}{qA^*TS} \right) \exp \left(\frac{q\Delta\phi}{\kappa_B T} \right) \quad (3)$$

where k_B and q are the Boltzmann constant and the electric charge, respectively; A^* Richardson constant; T is the absolute temperature; S is the contact area; and $\Delta\phi$ is the difference in barrier height. The contact area between the graphene and the substrate increases with as the r_c of graphene decreases, as shown in formula 3. Therefore, the contact resistance r_c of the interface between the graphene and Si substrate can be determined by the contact area. Based on formula 3 and the experimental resistance results of the emitter, it is clear that as the interface resistance decreased, the interface provided additional electrons for tunneling. At the same time, as the resistance of the emitter decreased, the emitter also provided additional electrons for easy transport. Therefore, as the series resistance decreases, the field emission properties can be improved dramatically.

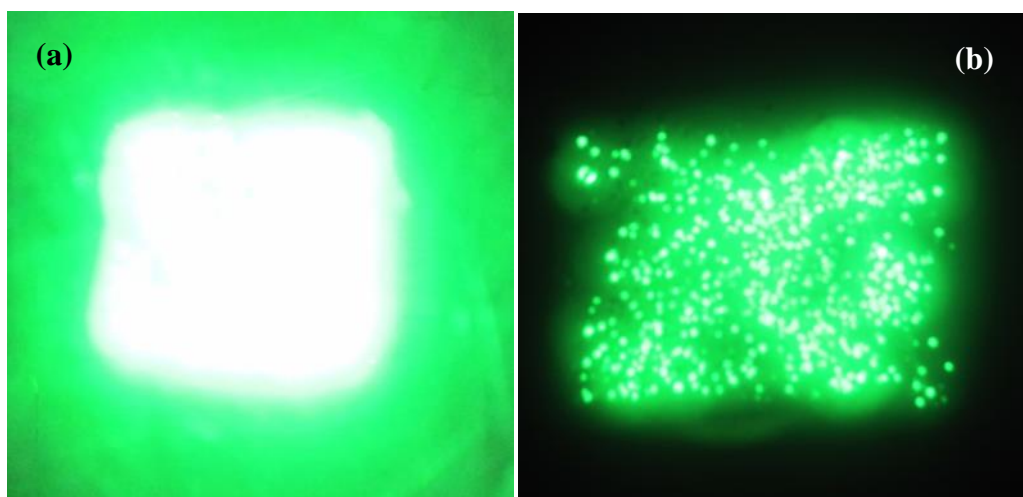


Figure 7. The emission images of (a) Cu nanoparticle/graphene composite and (b) pristine graphene emitters.

Field emission images for the Cu/graphene composite and pristine graphene are shown in Figure 7(a) and (b), which were obtained at an electrical field of $4.0 \text{ V}/\mu\text{m}$. A bright and high luminance intensity can be observed for the Cu/graphene composite emitter. However, for pristine graphene, a low luminance intensity and sparse emission dots appeared, as shown in Figure 7 (b). For the Cu/graphene composite emitter, the additional emitting sites and low series resistance resulted in an increased luminance intensity and improved emitting uniformity. In addition, during the field emission process, the Cu nanoparticles protected the graphene emitters from ion bombardment, which can enhance the stability of the emission. For the pristine graphene, the limited number of emission sites and the high series resistance resulted in poor field emission properties. As we know, a large voltage drop can occur due to a high resistance. Therefore, the voltage for electron field emission can be largely decreased. Therefore, a low luminance intensity and low number of emission locations were observed for the pristine graphene in Figure 7(b).

In recent years, graphene or carbon nanotube composite field emitters have been fabricated by many researchers [44-47] using CVD, chemical synthesis, and magnetron sputtering techniques, for example. Table 1 shows the field emission parameters of different carbon-based composite emitters

fabricated by different methods. From Table 1, it can be seen Cu/Graphene composite emitters that were fabricated by EPD exhibited a low turn-on field, low threshold and high field enhancement factor. Compared with that for other composite field emitters, our Cu/GP composite emitters have an appealing field emission performance, and the fabrication method for our vertical GP edges and tips is straightforward.

Table 1. Turn-on fields (V/ μm), threshold fields (V/ μm) and field enhancement factors for carbon-based nanoparticle composite field emitters fabricated by different methods in recent years.

| Particles/GP composite | TOF | TF | FEF (β) | Ref. |
|----------------------------|-------------------------------------|-----------------------------------|-----------------|------|
| Sn/Graphene | 2.1 (10 $\mu\text{A}/\text{cm}^2$) | 3.9 (1 mA/cm^2) | 1800 | 44 |
| Cu/Graphene | 1.9(10 $\mu\text{A}/\text{cm}^2$) | 3.4 (1 mA/cm^2) | 2600 | 27 |
| SnO ₂ /Graphene | 4.14(1 $\mu\text{A}/\text{cm}^2$) | 9.4 (1 mA/cm^2) | 979 | 45 |
| In/Carbon nanotube | 2.0 (10 $\mu\text{A}/\text{cm}^2$) | 3.9 (1 mA/cm^2) | 2706 | 46 |
| ZnO/Carbon nanotube | 1.5(0.1 $\mu\text{A}/\text{cm}^2$) | 2.9 (1 mA/cm^2) | 5741 | 47 |
| Present work | 1.55(10 $\mu\text{A}/\text{cm}^2$) | 2.45 (1 mA/cm^2) | 5600 | - |

4. SUMMARY AND CONCLUSION

In conclusion, the optimized field emission performance of graphene with a low turn-on field, a low threshold field and a high field enhancement factor was achieved by a one-step EPD process that introduced metallic particles onto graphene sheets. The synergistic effect of the Cu nanoparticles and graphene sheets in the Cu/graphene composite resulted in a high field emission current density and increased luminance intensity. It was concluded that Cu nanoparticles mainly increased the density of the field emission sites and optimized the contact interface resistance and conductivity of the graphene. This research indicated that the field emission of graphene could be optimized by Cu nanoparticles, and this method could be used for the development of efficient graphene-based composite field emitters.

ACKNOWLEDGMENTS

The authors would like to appreciate the financial supports of the National Natural Science Foundation of China (No. 51402077).

References

1. H. X. Chang, and H. K. Wu, *Adv. Funct. Mater.*, 23 (2013) 1984.
2. L.F. Chen, H. Yu, J.S. Zhong, J. Wu, and W.T. Su, *J. Alloys Compd.*, 749 (2018) 60.
3. C. Li, M. T. Cole, W. Lei, K. Qu, K. Ying, Y. Zhang, A. R. Robertson, J. H. Warner, S. Y. Ding, X. B. Zhang, B. P. Wang, and W. I. Milne, *Adv. Funct. Mater.*, 24 (9) (2014)1218.
4. C. K. Huang, Y. X. Ou, Y. Q. Bie, Q. Zhao, and D. P. Yu, *Appl. Phys. Lett.*, 98 (2011) 263104.
5. L.F. Chen, H. Yu, J.S. Zhong, J. Wu, and W.T. Su, *Mater. Sci. Eng. B.*, 220 (2017) 44.
6. F. J. Wang, L. N. Deng, and J. H. Deng, *Appl. Sur. Sci.*, 355 (2015) 218.
7. Y. Zhang, J. L. Du, S. Tang, P. Liu, S. Z. Deng, J. Chen, and N. S. Xu, *Nanotechnology* , 23 (2012) 015202.
8. Y. F. Guo, and W. L. Guo, *J. Phys. Chem. C.*, 117 (2013) 692.
9. Y. Wang, Y. M. Yang, Z. Z. Zhao, C. Zhang, and Y. H. Wu, *Appl. Phys. Lett.*, 103 (2013) 033115.

10. S.W. Lee, S.S. Lee, and E.-H. Yang, *Nanoscale Res. Lett.*, 4 (2009) 1218.
11. Z.M. Xiao, J.C. She, S.Z. Deng, Z.K. Tang, Z.B. Li, J.M. Lu, and N.S. Xu, *ACS Nano*, 4 (11) (2010) 633.
12. H. Yamaguchi, K. Murakami, X.G. Eda, T. Fujita, P.F. Guan, W.C. Wang, C. Gong, J. Boisse, S. Miller, M. Acik, and K. Cho, *ACS Nano*, 5 (6) (2011) 4945.
13. C.Y. Li, Z. Li, H.W. Zhu, K.L. Wang, J.Q. Wei, X. Li, P.Z. Su, H. Zhang, and D.H. Wu, *J. Phys. Chem. C.*, 114 (2010) 14008.
14. A.T.T. Koh, T. Chen, L. Pan, Z. Sun, and D.H.C. Chua, *J App Phys.*, 113 (2013) 174909.
15. T.K. Hong, D.W. Lee, H. J. Choi, H.S. Shin, and B.S. Kim, *ACS Nano*, 4 (2010) 3861.
16. T.T. Baby, and R. Sundara, *Mater; Chem. Phys.*, 135 (2012) 623.
17. L.F. Chen, H. He, D. Lei, Q. Menggen, L.Q. Hu, and D.R. Yang, *Appl. Phys. Lett.*, 103 (2013) 233105.
18. W. I. Park, C. H. Lee, J. M. Lee, N. J. Kim, and G. C. Yi, *Nanoscale*, 3 (2011) 3522.
19. X. Huang, X. J. Qi, F. Boey, and H. Zhang, *Chem. Soc. Rev.*, 41 (2012) 666.
20. S. Stankovich, D. A. Dikin, G. H. B. Dommett, K. M. Kohlhaas, E. J. Zimney, E. A. Stach, R. D. Piner, S. T. Nguyen, and R. S. Ruoff, *Nature* 442 (2006) 282.
21. X.E. Zhao, P. P. Zhang, Y. T. Chen, Z. Q. Su, and G. Wei, *Nanoscale*, 7 (2015) 5080.
22. N. Li, M. H. Cao, and C. W. Hu, *Nanoscale*, 4 (2012) 6205.
23. F. Schwierz, *Nat Nanotechnol.*, 5 (2010) 487.
24. Z. J. Fan, J. Yan, L. J. Zhi, Q. Zhang, T. Wei, J. Feng, M. L. Zhang, W. Z. Qian, and F. Wei, *Adv. Mater.*, 22 (2010) 3723.
25. P. T. Yin, T. H. Kim, J. W. Choi, and K. B. Lee, *Phys. Chem. Chem. Phys.*, 15 (2013) 12785.
26. L. F. Chen, H. Yu, J. S. Zhong, H. He, and T. Zhang, *Electrochim. Acta.*, 178 (2015) 732.
27. X. D. Hong, D. Liang, P.Z. Wu, and H.R. Zheng, *Diam & Relat Mater.*, 69 (2016) 61.
28. L.F. Chen, Z.G. Ji, Y.H. Mi, H.L. Ni, and H.F. Zhao, *Phys Scripta*, 82 (2010) 035602.
29. G.H. Chen, D.H. Shin, T. Iwasaki, H. Kawarada, and C.J. Lee, *Nanotechnology*, 19 (2008) 415703.
30. A.V. Kukhta, A. G. Paddubskaya, P. P. Kuzhir, S. A. Maksimenko, S. A. Vorobyov, S. Bistarelli, A. Cataldo, and S. Bellucci, *Synthetic Met.*, 222 (2016) 192.
31. R. Zan, U. Bangert, Q. Ramasse, and K.S. Novoselov, *J. Phys. Chem. Lett.*, 3 (2012) 953.
32. Q. Li, W.L. Zhu, J.J. Fu, H.Y. Zhang, G. Wu, and S.H. Sun, *Nano Energy*, 24 (2016) 1.
33. L. Jin, G.Y. He, J.J. Xue, T.T. Xu, and H.Q. Chen, *J Clean Prod.*, 161 (2017) 655.
34. M. Ahmed, M. J. Uddin, M. A. Rahman, N. Kishi, and T. Soga, *J. Cryst. Growth*, 449 (2016) 156.
35. C.C. Yeh, P.R. Wu, and D.H. Chen, *Mater. Lett.*, 136 (2014) 274.
36. Z.B. Su, L. Tan, R.Q. Yang, Y. Zhang, J. Tao, N. Zhang, and F.S. Wen, *Chem. Phys Lett.*, 695 (2018) 153.
37. R. H. Fowler, L. Nordheim, *Proc. R. Soc. London, Ser. A.*, 119 (1928) 173.
38. J. H. Zhang, C. R. Yang, W. W. Yang, T. Feng, X. Wang, and X. H. Liu, *Solid State Commun*, 138 (2006) 13.
39. J. H. Zhang, X. Wang, W. W. Yang, W. D. Yu, T. Feng, Q. Li, X. H. Liu, and C. H. Yang, *Carbon*, 44 (2006) 418.
40. L.F. Chen, H. He, H. Yu, Y.Q. Cao, D. Lei, Q. Menggen, C.X. Wu, and L.Q. Hu, *J. Alloys Compd.*, 610 (2014) 659.
41. O. Yaglioglu, A.J. Hart, R. Martens, and A.H. Slocum, *Rev Sci Instrum*, 77 (2006) 095105.
42. L.F. Chen, L. Wang, X.G. Yu, S.J. Zhang, D. Li, C. Xu, L.S. Zeng, S. Zhou, J.J. Zhao, F. Guo, L.Q. Hu, and D.R. Yang, *Appl. Sur. Sci.*, 265 (2013) 187.
43. S.C. Lim, J.H. Jang, D.J. Bae, G.H. Han, S. Lee, I.S. Yeo, and Y.H. Lee, *Appl. Phys. Lett.*, 95 (2009) 264103.
44. Z.J. Li, B.C. Yang, G.Q. Yun, S.R. Zhang, M. Zhang, M.X. Zhao, *J. Alloys Compd.* 550 (2013) 353.
45. J.J. Ding, X.B. Yan, J. Li, B.S. Shen, J. Yang, J.T. Chen, and Q.J. Xue, *ACS Appl. Mater. Inter.*

2011, 3, 4299.

46. M. Sreekanth, S. Ghosh, P. Biswas, S. Kumar, and P. Srivastava, *Appl. Sur. Sci.* 383 (2016) 84.

47. J. Kennedy, F. Fang, J. Futter, J. Leveneur, P.P. Murmu, G.N. Panin, T.W. Kang, and E. Manikandan, *Diam & Relat Mater.* 71 (2017) 79.

© 2020 The Authors. Published by ESG (www.electrochemsci.org). This article is an open access article distributed under the terms and conditions of the Creative Commons Attribution license (<http://creativecommons.org/licenses/by/4.0/>).